Chemically Resolved Interface Structure of Epitaxial Graphene on SiC(0001)

Jonathan D. Emery,[1] Blanka Detlefs,[2] Hunter J. Karmel,[1] Luke O. Nyakiti,[3] D. Kurt Gaskill,[3] Mark C. Hersam,[1,4] Jörg Zegenhagen,[2] and Michael J. Bedzyk[1,5,*]

[1]*Department of Materials Science and Engineering, Northwestern University, Evanston, Illinois 60208, USA*
[2]*European Synchrotron Radiation Facility, BP 220, 38043 Grenoble, Cedex 9, France*
[3]*US Naval Research Laboratory, Washington, District of Columbia 20375, USA*
[4]*Department of Chemistry, Northwestern University, Evanston, Illinois 60208, USA*
[5]*Department of Physics and Astronomy, Northwestern University, Evanston, Illinois 60208, USA*

(Received 25 July 2013; published 19 November 2013)

Atomic-layer 2D crystals have unique properties that can be significantly modified through interaction with an underlying support. For epitaxial graphene on SiC(0001), the interface strongly influences the electronic properties of the overlaying graphene. We demonstrate a novel combination of x-ray scattering and spectroscopy for studying the complexities of such a buried interface structure. This approach employs x-ray standing wave-excited photoelectron spectroscopy in conjunction with x-ray reflectivity to produce a highly resolved chemically sensitive atomic profile for the terminal substrate bilayers, interface, and graphene layers along the SiC[0001] direction.

DOI: 10.1103/PhysRevLett.111.215501 PACS numbers: 61.48.Gh, 61.05.cm, 68.49.Uv, 79.60.−i

Epitaxial graphene (EG) grown on the Si-terminated face of silicon carbide [SiC(0001)] is of interest due to its unique physical properties [1,2], potential in numerous applications [3–5], and amenity for wafer-scale fabrication [6,7]. EG/SiC(0001) production proceeds *via* preferential Si sublimation and reconstruction of the surface C to yield a heterostructure that exhibits the technologically relevant properties characteristic of graphene, such as the Dirac cone band structure [8,9] and large room-temperature Hall mobilities [1,6]. As such, EG/SiC(0001) is a comparatively viable option for the large-scale production of graphene. However, despite the advancement in both fundamental understanding and practical application of the material, there remains much unknown about the structure and behavior of EG/SiC(0001), particularly concerning the influence of the EG/SiC(0001) interface on the properties of the overlaying graphene.

Early studies revealed that EG/SiC(0001) possesses a complex $6\sqrt{3} \times 6\sqrt{3}R30°$ ($6R3$) reconstructed interfacial layer [10], referred to herein as the interfacial, or EG_0, layer. This layer has significant influence on the growth, morphology, and electronic behavior of the overlaying graphene [8,11–14]. It has been contentiously debated as the cause of EG/SiC(0001) symmetry breaking and band gap opening [15,16], and has been identified as a primary source for carrier doping and scattering in the graphene layers [17,18]. Work on H-intercalated graphene transistors highlights the influence of this layer on the electronic properties of the overlaying graphene, demonstrating that physically decoupling the EG_0 layer from the substrate improves properties critical to graphene-based transistor performance [19,20]. A precise understanding of the structure of EG/SiC(0001) is therefore not only fundamentally important, but is also central to the prospects of graphene engineering and functionalization.

Because of the importance of the interfacial layer to the behavior of EG/SiC(0001), there have been numerous efforts to characterize its structure, including low-energy electron diffraction [10,13], scanning-tunneling microscopy, [21–23], x-ray photoemission spectroscopy (XPS) [24,25], x-ray reflectivity (XRR) [26], and cross-sectional transmission electron microscopy [27,28]. These experimental reports, combined with computational studies [14,29,30], have generated a multitude of interfacial models. These include those with weak [10] or strong [12,14,25,29] substrate-interlayer coupling, C-rich [14,23,25] or Si-rich interfacial structures [21,26], or significant populations of Si dangling bonds [12,29]. However, despite this persistent incongruence, it is now understood that the interface consists of a corrugated, topologically graphenelike layer which, due to its coupling with the underlying SiC, lacks the electronic properties of pristine graphene [25,31].

In this Letter we detail the structure of the interface by employing a suite of x-ray characterization techniques, including depth-sensitive XPS, x-ray standing wave-enhanced XPS (XSW-XPS), and x-ray reflectivity (XRR). These tools, when employed collectively, provide the chemically specific structural information necessary to clarify previously unknown details of the EG/SiC(0001) interface. This approach ultimately enables the construction of a chemically resolved interfacial map with sub-Å resolution along the SiC[0001] direction.

The XSW technique affords conventional photoelectron spectroscopy with high spatial resolution due to the influence of the XSW [here produced by the SiC(0006) Bragg reflection] on the photoabsorption process. A depiction of this phenomenon is shown in Fig. 1. The XSW phase can be adjusted relative to the atomic planes by tuning the incident beam energy (E_γ) within the range of the Bragg reflection, which in turn modulates the x-ray photoelectron yields of

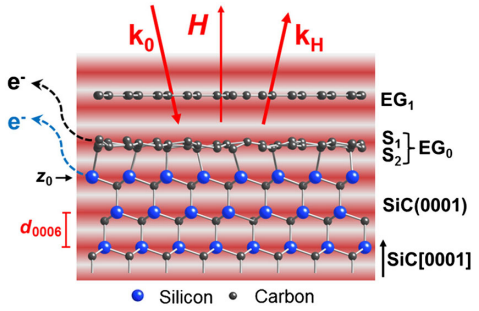

FIG. 1 (color online). Schematic of the XSW generated by the 6*H*-SiC(0006) Bragg reflection (period of $d = 2.52$ Å). The incident and reflected plane waves (wave vectors $\mathbf{k_0}$ and $\mathbf{k_H}$, respectively) interfere to produce a standing wavefield (antinodes shaded red).

atoms within the field. Depending on the spatial distribution of these atoms with respect to the substrate, this process produces distinct photoemission yield modulations as a function of E_γ. XSW data analysis determines two model-independent fit parameters, f_j and P_j, which are the amplitude and phase of the $H = 0006$ Fourier component of the jth chemically sensitive atomic density profile. For details, see the Supplemental Material [32] and Ref. [33].

In this work we will assume a normalized Gaussian distribution for each XPS-selected atomic layer. The (0006) Fourier component is therefore

$$F_j = f_j e^{2\pi i P_j} = e^{-2\pi^2\sigma_j^2/d^2} e^{2\pi i z_j/d}. \quad (1)$$

For this model, the XSW-measured Fourier amplitude f_j determines the Gaussian width σ_j, and the measured phase, $P_j = z_j/d$ $(0 \le P_j < 1)$, determines the mean height z_j (*modulo-d*) of the jth atomic layer relative to the substrate unit cell origin z_0 (Fig. 1). Because of the *modulo-d* ambiguity and potential contributions to P_j from multiple atomic layers, we supplement this analysis with high-resolution XRR (see Ref. [34] and references therein), a measurement that is sensitive to electron density distributions over a larger spatial extent.

EG/SiC(0001) samples of 1.3 and 0.5 monolayer (ML of graphene = 38.2 C/nm^2) graphene coverage (Θ_T) were prepared by thermal decomposition of 6*H*-SiC(0001) substrates in ultrahigh vacuum (UHV) at 1200–1300 °C. Results for the 1.3 ML sample are presented in the main text. Complimentary analysis of the 0.5 ML sample, as well as an Ar-grown sample of 1.7 ML coverage, are provided in the Supplemental Material [32] to confirm and generalize the conclusions of the main text. Prior to measurements, the samples were annealed in UHV at ~600 °C, and the presence of the 6*R*3 interface was verified with low-energy electron diffraction. Further sample preparation details are provided in the Supplemental Material [32].

XSW-XPS measurements were performed in UHV at the ID32 beam line of the European Synchrotron Radiation Facility. Working near the SiC(0006) Bragg back-reflection condition ($\theta_B \sim 88°$), the incident beam energy and FWHM bandwidth were $E_\gamma = E_B = 2450$ and $\Delta E_\gamma = 0.34$ eV, respectively. The total FWHM resolution of the spectrometer was 0.6 eV. To vary the depth sensitivity, the photoemission angle (α) was set to either 78° or 2°, as shown in Fig. 2. The grazing ($\alpha = 2°$) emission geometry was used during XSW experiments. XRR data were acquired at 5ID-C at the Advanced Photon Source. XRR integrated signal intensity was extracted following the methods described in Ref. [34]. XRR data fitting was limited to the region $1.2 < L < 14.0$, where $L = (c_{\mathrm{SiC}} q_z)/(2\pi)$ is the SiC reciprocal lattice index, $q_z = 4\pi \sin(2\theta/2)/\lambda$ is the out-of-plane component of the momentum transfer vector, 2θ is the scattering angle, λ is the x-ray wavelength, and $c_{\mathrm{SiC}} = 15.12$ Å is the lattice constant for 6*H*-SiC.

Figure 2 presents depth-sensitive (effective probing depth Λ_{eff}) core-level photoelectron spectra used to identify near-surface C and Si chemical species. When measured at emission angle $\alpha = 78°$ [Figs. 2(a) and 2(b)], the Si 1*s* and C 1*s* spectra are dominated by bulk SiC components with binding energies (BE) of 1841.6 ± 0.1 and 283.8 ± 0.1 eV, respectively. The C 1*s* spectrum possesses additional high-energy core-shifted components from graphene and interfacial layers, as previously investigated [22,24,25]. The Si 1*s* spectrum, in contrast, appears to consist of a single component. By reducing α to 2°, Λ_{eff} is reduced from nm to Å scale [Figs. 2(c) and 2(d)]. A comparison of the C 1*s* spectra in Figs. 2(a) and 2(c) reveals strong attenuation ($\times 1/30$) of the $\mathrm{C_{Bulk}}$ integrated signal with respect to the higher BE spectral components.

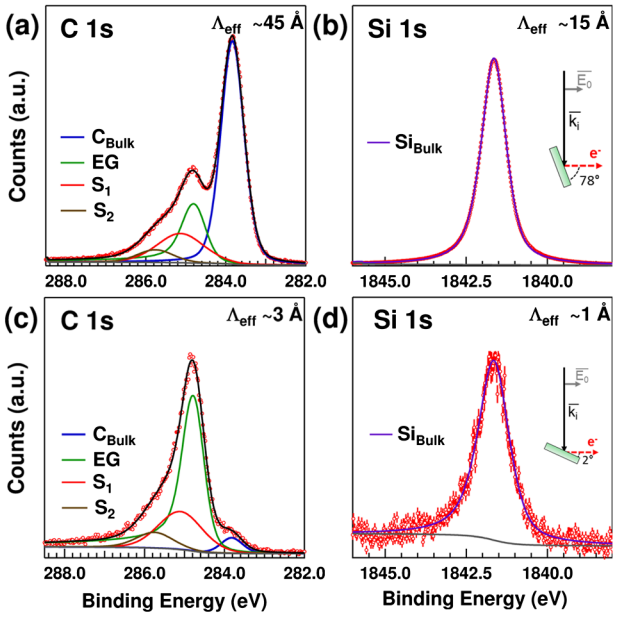

FIG. 2 (color online). C 1*s* and Si 1*s* photoelectron spectra for 1.3 ML EG/SiC(0001). $\mathrm{Si_{Bulk}}$, $\mathrm{C_{Bulk}}$, EG, S_1, and S_2 components are shown in purple, blue, green, red, and brown, respectively. (a)–(b) Data collected at emission angle $\alpha = 78°$. (c)–(d) Data collected with a highly surface-sensitive geometry ($\alpha = 2°$).

In contrast, no distinguishable surface-specific component is present in the $\alpha = 2°$ Si 1s spectrum [Fig. 2(d)].

We identify three distinct C 1s surface species, labeled in Figs. 2(a) and 2(c) as EG, S_1, and S_2. These components are shifted in BE by +0.95, +1.35, and +1.95 eV with respect to the C_{Bulk} peak, and have resolution-broadened FWHMs of 0.7, 1.0, and 1.1 eV. The EG component arises from the graphene layers, and the S_1 and S_2 components belong to species within the interfacial layer. The Si 1s spectra are fit with a single, slightly asymmetrically broadened line shape [Figs. 2(b) and 2(d)]. When the geometry is more highly surface sensitive the peak broadens by ~20%, as would be consistent with the increased relative contribution of strained, near-surface Si-C bonds possessing a variety of bonding configurations due to interactions between terminal Si species and C within the interfacial layer.

Using the XPS peak-fitting models described above, we extract the chemically specific, E_γ-dependent XSW photoemission yields (Fig. 3). Each of the five measured components exhibits a distinct XSW modulation, demonstrating that each chemical species possesses a distinct distribution profile along the SiC[0001] direction. Results from least-squares fitting of the yield equation [32,33] to the data are overlaid for each component in Fig. 3. All best-fit f_j and P_j values are reported in Table I.

The Fourier phases for both Si_{Bulk} and C_{Bulk} indicate that these species are centered at their nominal SiC positions (equal to 0.00 and −0.25, respectively). However, small deviations of XSW best-fit results for both species from the ideal Si_{Bulk} and C_{Bulk} values (−0.05 and +0.05 Å, respectively) imply the possibility of small displacements. The Fourier amplitude $f_{C_{Bulk}} = 1.0 \pm 0.1$ denotes essentially perfect C_{Bulk} coherency with the substrate. Conversely, the Si_{Bulk} result ($f_{Si_{Bulk}} = 0.8 \pm 0.1$) suggests a broader-than-ideal distribution for Si atoms within the topmost SiC bilayers ($\sigma_{Si_{Bulk}} = 0.3 \pm 0.1$ Å, as compared to the bulk ~0.1 Å thermal vibrational amplitude for SiC at room temperature).

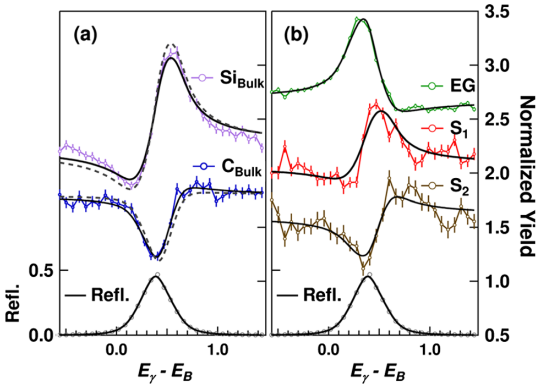

FIG. 3 (color online). XSW results for (a) near-surface bulk and (b) surface species corresponding to XPS components in Figs. 2(c) and 2(d). Measured (gray circles) and fitted (black) reflectivity from the SiC(0006) Bragg peak are plotted vs energy offset from the geometrical Bragg condition ($E_B = 2450$ eV). Normalized yields and best-fit results (black) are offset for clarity, and simulated yields for ideal SiC bulk are in dashed black.

The results for the S_1 and S_2 components are shown in Fig. 3(b). Converted to absolute positions [Eq. (1)], the S_1 and S_2 components reside at $z_{S_1} = 2.39 \pm 0.13$ and $z_{S_2} = 2.07 \pm 0.10$ Å above the terminal Si layer. In addition, a comparison of the Fourier amplitudes of the interfacial species reveals a smaller value for S_1, indicating that σ_{S_1} is significantly broader in comparison to σ_{S_2}.

The remaining C 1s component arises from atoms located in the EG overlayers. Because EG/SiC(0001) does not grow in a single, uniform monolayer [6], single-layer XSW modeling is inappropriate. Instead, the f_{EG} and P_{EG} values are determined from the superposition of contributions from $k > 1$ atomic layers of graphene. Here, the long-range structural information lacking in XSW is provided by XRR, thereby enabling the exploration of models with varying EG layer coverage.

XRR data are analyzed by comparing measured reflectivity values to those calculated from a model consisting of k atomic layers, each described by layer occupancy (Θ_k), position (z_k), and distribution width (σ_k) [26,34]. In this work, we are able to constrain the XRR analysis using XSW results (within 1-sigma confidence levels), thereby mitigating ambiguities that commonly arise during model-based XRR fitting. For Si_{Bulk} and C_{Bulk}, we allow for the slight broadening and displacement of bulk-positioned atoms within the three topmost SiC bilayers. Importantly, XSW interpretation of the S_1 and S_2 signals constrains these two components into single, well-defined interfacial distributions.

The XSW-constrained XRR result is shown in Fig. 4(a). The fit finds the EG_1, EG_2, and EG_3 layers positioned at 5.82, 9.17, and 12.57 Å above the terminal Si layer with respective coverages (Θ_k) of 0.86, 0.45, and 0.03 ML. The widths of the graphene layers (Table I), monotonically decrease as a function of distance from the interface, in close agreement with trends observed in Refs. [13,26]. The S_1 and S_2 layer positions converge to $z_{S_1} = 2.45$ and

TABLE I. XSW-measured values, P_j and f_j, for the jth chemical species. The absolute positions (z_j), widths (σ_j), and coverages (Θ_j) are derived using combined x-ray analysis. Uncertainties on the last significant figures are reported in parentheses.

j		P_j	z_j(Å)	f_j	σ_j(Å)	[a]Θ_j(MLs)
EG	EG_3		12.57		0.05	0.03
	EG_2	0.42(2)	9.16	0.48(5)	0.11	0.45
	EG_1		5.82		0.21	0.86
S_1		0.95(5)	2.4(1)	0.4(2)	0.5(1)	0.70
S_2		0.82(4)	2.1(1)	0.9(2)	0.2(1)	0.27
Si_{Bulk}		−0.02(2)	−0.05(5)	0.8(1)	0.3(1)	0.28
C_{Bulk}		−0.23(2)	−0.58(5)	1.0(1)	0.1(1)	0.34

[a]Based on EG, 1 ML = 38.2 atoms/nm^2.

$z_{S_2} = 2.13$ Å, respectively, well within the 1-sigma confidence levels derived from XSW analysis. The topmost bulk Si layer is ~15% depleted, which is presumably a growth artifact from the Si sublimation and corroborates the observation of near-surface Si vacancies [35]. This Si depletion limits the maximum number of sp^3-hybridized C atoms to ~25% of the atoms within the graphenelike interfacial layer. Finally, the C atoms in the topmost SiC bilayers are found to relax outward by, on average, 0.04 Å, consistent with the XSW result (0.05 ± 0.05 Å). With these results it is possible to compute the XRR-derived complex (0006) geometrical structure factor for the EG layers,

$$S_{\mathrm{EG}} = \frac{1}{\Theta_T} \sum_{k=1}^{3} \Theta_k e^{2\pi i z_k/d} e^{-2\pi^2 \sigma_k^2/d^2}, \qquad (2)$$

and thereby back-calculate the amplitude, $f_{\mathrm{EG}} = |S_{\mathrm{EG}}| = 0.49$ and phase, $P_{\mathrm{EG}} = \mathrm{Arg}(S_{\mathrm{EG}})/2\pi = 0.41$. These XRR values match closely with the XSW-derived values for EG, a testament to the exactitude and self-consistency of the model and analysis.

The resultant chemically sensitive atomic density profile $[N_a(z)]$ is shown in Fig. 4(b), and interfacial region detail is shown in Fig. 4(c). From this construction we conclude that the interfacial region contains a broad, C-only layer with graphenelike (0.97 ± 0.05 ML) atomic density. Within this layer there exist two chemically distinct C species. The S_2 species, which has the highest BE [Fig. 2(c)], accounts for ~25% of the interfacial C and is located 2.1 ± 0.1 Å above the terminal Si layer. This displacement is only 0.2 Å larger than the nominal Si-C bond distance of 1.9 Å in SiC, indicating the partial sp^3 hybridization of the interfacial layer with substrate. The narrower distribution width of the S_2 species ($\sigma_{S_2} = 0.2 \pm 0.1$ Å) closely agrees with that of the topmost Si layer (0.3 ± 0.1 Å), suggesting strong coherency between the two layers. Furthermore, the coverage ratio for the topmost Si layer to S_2 is ~1:1 (Table I). These findings imply that each Si atom in the topmost SiC bilayer is chemically bonded to an interfacial S_2 atom and substantiates the claim that there exist essentially no unsaturated Si dangling bonds at the interface [25].

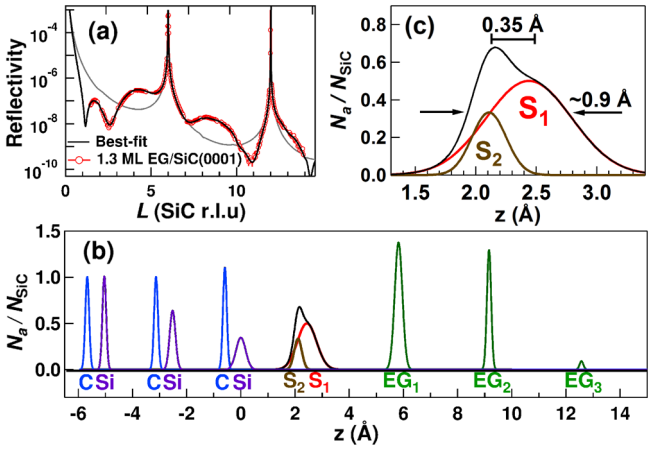

FIG. 4 (color online). (a) XSW-constrained x-ray reflectivity results for 1.3 ML EG/SiC(0001). The best fit (black) to the data (red) is shown together with a simulated bulk-truncated SiC curve (gray). (b) The atomic density map derived from combined XSW-XPS and XRR analysis. (c) The interfacial detail shows two interfacial components, S_1 and S_2, separated by ~0.35 Å, to form a ~0.9 Å wide, low-areal density interface layer.

The S_1 species, which accounts for the other 75% of the interfacial C, is positioned 2.4 ± 0.1 Å above the topmost Si layer and possesses a significantly larger distribution width ($\sigma_{S_1} \sim 0.5$ Å) as compared to the S_2 species. This broadening reduces the maximum areal density at the center of the interfacial layer and is consistent with the observations of a highly corrugated interfacial layer [2,14,22,30] as well as the reduced effective interfacial atomic density, as seen with cross-sectional transmission electron microscopy [27,28]. This broadening also points to multiple degrees of strain in the bonding configurations for the S_1 carbons, which is consistent with our finding of a slightly broader spectral width for the fitted S_1 XPS peak [32].

Our analysis yields no evidence for a number of other proposed interfacial structures. Specifically, Refs. [21,26] suggest the presence of large populations of interfacial Si atoms. These models prove inconsistent with our combined x-ray analysis. First, we find no spectroscopic evidence of nonbulk Si species, particularly from Si tetramers or other Si adatoms, which would exhibit negatively core-shifted Si 1s components with respect to the SiC signal due to the presence of Si-Si bonds. Instead, the depletion of Si in the topmost SiC bilayers suggests the presence of negatively charged Si vacancies [36], which may play a role in the n-type doping of the graphene layers. With respect to the difference in interpretation of the XRR presented herein and that of Ref. [26], we note that, because model-based fitting of XRR data often leads to numerous statistically equivalent solutions, unambiguous analysis typically requires complimentary information. Our approach benefits from constraints provided by the structurally sensitive XSW-XPS measurement and finds that the XRR data can be well fit with a C-only interfacial layer with graphenelike density, therefore generally supporting the models of Emtsev [25], Kim [14], and Varchon [30]. With respect to the discrepancy in XPS peak fitting between this work and that of Ref. [25], we note the following: (i) the model in Ref. [25] does not account for the probable existence of sub-ML EG inclusions in their nominally zero-layer graphene, and (ii) there are a large number of potential influences (e.g., bond-charge transfer, spontaneous substrate polarization [17], defect states [23], charge-transfer doping [25], band bending [19], and sp^2 vs sp^3 hybridization) on the precise binding energies of the interfacial species, making the identification of chemical species from peak shifts alone tenuous. Regardless, the binding energies that we find for $S_1 (= \mathrm{BE_{EG}} + 0.4\,\mathrm{eV})$ and $S_2 (= \mathrm{BE_{EG}} + 1.0\,\mathrm{eV})$ are in accordance with those expected from sp^2- and sp^3-hybridized species, respectively, and are strongly supported by XSW analysis.

In summary, we have combined depth-sensitive XPS, XSW-XPS, and XRR to create a structural profile of the EG/SiC(0001) interface with unprecedented chemical and spatial resolution. The high degree of consistency between the two sub-Å resolution measurements provides compelling evidence for the validity of our structural model and overall methodology. The interfacial layer, which has an influential role in the electronic behavior of EG/SiC(0001), and, consequently, in graphene-based devices, consists solely of C, possessing two distinct chemical species located at 2.1 and 2.4 Å above the topmost Si layer of the SiC. Our results support the strongly interacting interfacial layer model and rule out any significant presence of Si species in adatom structures or within the interfacial layer. In perspective, XSW-XPS and XRR may prove an effective tool for the study of the complex interfaces that exist in emerging 2D crystals and heterostructures, including intercalated, doped, and functionalized EG/SiC nanostructures.

We acknowledge support from MRSEC (NSF Grant No. DMR-1121262) and the Office of Naval Research for the support of the NRL, H. J. K., and M. C. H. through Grant No. N00014-11-1-0463. M. C. H also acknowledges the Keck Foundation. We acknowledge use of ID32, ESRF, and DND-CAT, APS (DOE Award No. DE-AC02-06CH11357 to ANL). DND-CAT is supported by DuPont, Northwestern University, and Dow. We acknowledge use of X24A at NSLS (DOE Award No. DE-AC02-98CH10886 to BNL) for initial XSW measurements with assistance from Joseph Woicik (NIST). We acknowledge Denis Keane (DND-CAT) and Paul Fenter (ANL) for assistance with XRR measurements, Chip Eddy (NRL) for useful discussions on graphene synthesis, and Virginia Wheeler and Rachael Myers-Ward (NRL) for sample production.

*Corresponding author.
bedzyk@northwestern.edu

[1] C. Berger *et al.*, J. Phys. Chem. B **108**, 19 912 (2004).
[2] C. Berger *et al.*, Science **312**, 1191 (2006).
[3] Y.-M. Lin, C. Dimitrakopoulos, K. A. Jenkins, D. B. Farmer, H.-Y. Chiu, A. Grill, and P. Avouris, Science **327**, 662 (2010).
[4] Y.-M. Lin *et al.*, Science **332**, 1294 (2011).
[5] A. Tzalenchuk, S. Lara-Avila, A. Kalaboukhov, S. Paolillo, M. Syväjärvi, R. Yakimova, O. Kazakova, T. Janssen, V. Fal'Ko, and S. Kubatkin, Nat. Nanotechnol. **5**, 186 (2010).
[6] K. V. Emtsev *et al.*, Nat. Mater. **8**, 203 (2009).
[7] Y.-M. Lin, A. Valdes-Garcia, S.-J. Han, D. B. Farmer, I. Meric, Y. Sun, Y. Wu, C. Dimitrakopoulos, A. Grill, and P. Avouris, Science **332**, 1294 (2011).
[8] T. Ohta, A. Bostwick, J. L. McChesney, T. Seyller, K. Horn, and E. Rotenberg, Phys. Rev. Lett. **98**, 206802 (2007).
[9] S. Zhou, G.-H. Gweon, J. Graf, A. Fedorov, C. Spataru, R. Diehl, Y. Kopelevich, D.-H. Lee, S. G. Louie, and A. Lanzara, Nat. Phys. **2**, 595 (2006).
[10] A. J. Van Bommel, J. E. Crombeen, A. Van Tooren, Surf. Sci. **48**, 463 (1975).
[11] A. Bostwick, T. Ohta, T. Seyller, K. Horn, and E. Rotenberg, Nat. Phys. **3**, 36 (2006).
[12] F. Varchon *et al.*, Phys. Rev. Lett. **99**, 125805 (2007).
[13] C. Riedl, U. Starke, J. Bernhardt, M. Franke, and K. Heinz, Phys. Rev. B **76**, 374009 (2007).
[14] S. Kim, J. Ihm, H. J. Choi, and Y. W. Son, Phys. Rev. Lett. **100**, 176802 (2008).
[15] S. Y. Zhou, G. H. Gweon, A. V. Fedorov, P. N. First, W. A. De Heer, D. H. Lee, F. Guinea, A. H. C. Neto, and A. Lanzara, Nat. Mater. **6**, 916 (2007).
[16] E. Rotenberg, A. Bostwick, T. Ohta, J. L. McChesney, T. Seyller, and K. Horn, Nat. Mater. **7**, 258 (2008).
[17] J. Ristein, S. Mammadov, and T. Seyller, Phys. Rev. Lett. **108**, 246104 (2012).
[18] G. M. Rutter, J. N. Crain, N. P. Guisinger, T. Li, P. N. First, and J. A. Stroscio, Science **317**, 219 (2007).
[19] C. Riedl, C. Coletti, T. Iwasaki, A. A. Zakharov, and U. Starke, Phys. Rev. Lett. **103**, 246804 (2009).
[20] J. A. Robinson, M. Hollander, M. LaBella, K. A. Trumbull, R. Cavalero, and D. W. Snyder, Nano Lett. **11**, 3875 (2011).
[21] G. M. Rutter, N. P. Guisinger, J. N. Crain, E. A. A. Jarvis, M. D. Stiles, T. Li, P. N. First, and J. A. Stroscio, Phys. Rev. B **76**, 235416 (2007).
[22] W. Chen, H. Xu, L. Liu, X. Y. Gao, D. C. Qi, G. W. Peng, S. C. Tan, Y. P. Feng, K. P. Loh, and A. T. S. Wee, Surf. Sci. **596**, 176 (2005).
[23] Y. Qi, S. H. Rhim, G. F. Sun, M. Weinert, and L. Li, Phys. Rev. Lett. **105**, 085502 (2010).
[24] L. I. Johansson, F. Owman, and P. Martensson, Phys. Rev. B **53**, 13 793 (1996).
[25] K. V. Emtsev, F. Speck, T. Seyller, L. Ley, and J. D. Riley, Phys. Rev. B **77**, 155303 (2008).
[26] J. Hass, J. E. Millan-Otoya, P. N. First, and E. H. Conrad, Phys. Rev. B **78**, 205424 (2008).
[27] J. Borysiuk, R. Bozek, W. Strupinski, A. Wysmolek, K. Grodecki, R. Steapniewski, and J. M. Baranowski, J. Appl. Phys. **105**, 023503 (2009).
[28] X. J. Weng, J. A. Robinson, K. Trumbull, R. Cavalero, M. A. Fanton, and D. Snyder, Appl. Phys. Lett. **97**, 201905 (2010).
[29] A. Mattausch and O. Pankratov, Phys. Rev. Lett. **99**, 076802 (2007).
[30] F. Varchon, P. Mallet, J. Y. Veuillen, and L. Magaud, Phys. Rev. B **77**, 235412 (2008).
[31] S. Goler *et al.*, Carbon **51**, 249 (2013).
[32] See Supplemental Material at http://link.aps.org/supplemental/10.1103/PhysRevLett.111.215501 for supporting data and details on XSW and XPS modeling, sample preparation, experimental procedures, and analysis of complimentary samples.
[33] D. P. Woodruff, Rep. Prog. Phys. **68**, 743 (2005).
[34] J. D. Emery, Q. H. Wang, M. Zarrouati, P. Fenter, M. C. Hersam, and M. J. Bedzyk, Surf. Sci. **605**, 1685 (2011).
[35] X. Gao, S. Chen, T. Liu, W. Chen, A. T. S. Wee, T. Nomoto, S. Yagi, K. Soda, and J. Yuhara, Phys. Rev. B **78**, 201404 (2008).
[36] T. Wimbauer, B. K. Meyer, A. Hofstaetter, A. Scharmann, and H. Overhof, Phys. Rev. B **56**, 7384 (1997).